

# A ROBUST AND EFFICIENT MULTI-AGENT REINFORCEMENT LEARNING FRAMEWORK FOR TRAFFIC SIGNAL CONTROL

**Sheng-You Huang\***

National Yang Ming Chiao Tung University  
shengyouhuang.cs13@nycu.edu.tw

**Yen-Chi Chen**

Academia Sinica  
zxkyjimmy@gmail.com

**I-Hau Yeh**

ELAN Microelectronics Corporation  
ihyeh@emc.com.tw

**Chien-Yao Wang**

Academia Sinica  
kinyiu@iis.sinica.edu.tw

**I-Chen Wu**

National Yang Ming Chiao Tung University  
icwu@cs.nycu.edu.tw

**Hsiao-Chuan Chang\***

National Yang Ming Chiao Tung University  
s312581015.ii12@nycu.edu.tw

**Ting-Han Wei**

Kochi University of Technology  
tinghan.wei@kochi-tech.ac.jp

**Sheng-Yao Kuan**

ELAN Microelectronics Corporation  
shaun.kuan@emc.com.tw

**Hsuan-Han Lee**

ELAN Microelectronics Corporation  
henry.lee@emc.com.tw

*\* Equal Contribution.*

## ABSTRACT

Reinforcement Learning (RL) in Traffic Signal Control (TSC) faces significant hurdles in real-world deployment due to limited generalization to dynamic traffic flow variations. Existing approaches often overfit static patterns and use action spaces incompatible with driver expectations. This paper proposes a robust Multi-Agent Reinforcement Learning (MARL) framework validated in the Vissim traffic simulator. The framework integrates three mechanisms: (1) Turning Ratio Randomization, a training strategy that exposes agents to dynamic turning probabilities to enhance robustness against unseen scenarios; (2) a stability-oriented Exponential Phase Duration Adjustment action space, which balances responsiveness and precision through cyclical, exponential phase adjustments; and (3) a Neighbor-Based Observation scheme utilizing the MAPPO algorithm with Centralized Training with Decentralized Execution (CTDE). By leveraging centralized updates, this approach approximates the efficacy of global observations while maintaining scalable local communication. Experimental results demonstrate that our framework outperforms standard RL baselines, reducing average waiting time by over 10%. The proposed model exhibits superior generalization in unseen traffic scenarios and maintains high control stability, offering a practical solution for adaptive signal control.

**Key word:** Multi-agent RL, TSC optimization, CTDE

## INTRODUCTION

As urbanization accelerates globally, traffic congestion has evolved into a critical bottleneck restricting sustainable city development, causing severe economic losses and environmental degradation. According to the INRIX traffic report in 2025 (1), traffic congestion costs the U.S. economy over \$85 billion—an 11.3% increase from the previous year. Drivers in metropolitan areas continue to lose approximately 50 ~ 112 hours annually to delays, underscoring the

critical need for Advanced Traffic Management Systems (ATMS) to mitigate these severe economic and temporal losses. Traditional control methods rely on predefined rules and often lack the flexibility to handle the non-linear and stochastic nature of real-time traffic. Conversely, Deep Reinforcement Learning (DRL) enables agents to dynamically optimize signal policies, offering superior adaptability to fluctuating traffic demands.

Direct training in physical environments is prohibited by safety and cost constraints, making high-fidelity simulation indispensable. While most Reinforcement Learning Traffic Signal Control (RL-TSC) studies use SUMO (2) or CityFlow (3) for their efficiency, these platforms often rely on simplified models that lack realism. To bridge the 'sim-to-real' gap, this study uses PTV Vissim (4), the industry standard for microscopic traffic modeling. Addressing the scarcity of Vissim-based RL research due to complex integration barriers, we leverage the VissimRL framework (5) to seamlessly interface the RL agent with this high-fidelity environment.

Despite advanced simulation tools, real-world deployment faces three fundamental hurdles. First, regarding environmental generalization, agents must adapt to stochastic, non-stationary traffic flows without overfitting to static training patterns. Second, action space design requires balancing stability with responsiveness—maintaining safety-critical cyclic sequences while reacting agilely to congestion. Finally, centralized systems do not scale to larger traffic grids. A framework that can facilitate global cooperation through decentralized execution is necessary.

Thus, we propose a robust and stable Multi-Agent RL (MARL) framework for traffic signal control (TSC), with three specific technical improvements:

1. **Robustness via Turning Ratio Randomization:** We introduce a randomization training strategy to enhance the agent's robustness across non-stationary traffic conditions.
2. **Exponential Phase Duration Adjustment:** We propose a cyclic control mechanism with exponential adjustment steps to balance stability and reactivity via coarse-to-fine control.
3. **Scalable Coordination via Neighbor-Level Observation:** We employ a centralized training with decentralized execution (CTDE) framework to resolve the scalability and coordination dilemma through neighbor-level observations.

Experiment results demonstrate that our framework reduces average waiting time by over 10% in unseen scenarios, significantly enhancing robustness. Furthermore, our approach achieves robust coordination relying solely on scalable neighbor observations.

## BACKGROUND

This section establishes the theoretical foundation for our study. We first survey prior RL-based control methods, followed by the formalization of the TSC problem. Finally, we investigate the critical role of observation scope in large-scale network coordination.

### REINFORCEMENT LEARNING APPROACHES FOR TSC

Reinforcement Learning (RL) has been extensively investigated for Traffic Signal Control (TSC). Existing studies can be broadly categorized based on their training scenarios and action space formulations. However, while these approaches have achieved success in specific simulation settings, critical challenges regarding environmental generalization and control stability persist.

#### Training Scenarios and Generalization

A substantial body of research (6, 7) focuses on optimizing performance under static traffic conditions, where flow rates and turning ratios remain constant. Although this setup ensures stable

convergence for specific demand profiles, it often leads to overfitting the training distribution. Instead of learning the underlying traffic dynamics, agents tend to memorize specific timing patterns. Consequently, these models struggle to generalize to unseen scenarios, often requiring distinct policies for different time periods (e.g., peak vs. off-peak) to maintain performance. This limitation hinders real-world deployment, where traffic is non-stationary, necessitating a single robust model capable of handling diverse conditions without frequent retraining.

## Action Space Architectures

Action space design is critical for ensuring both the safety and stability of control policies. Existing approaches typically adopt either acyclic or cyclic control mechanisms.

Acyclic control (7, 8, 9, 10, 11) offers flexibility by allowing arbitrary phase selection but violates the fixed-sequence mandates essential for driver safety. Consequently, cyclic control is preferred for real-world deployment. Binary Switching methods (12, 13, 14) provides fine-grained control but often leads to unpredictable signal oscillation and high communication overhead. Direct Duration Setting methods (15, 16), although simple, frequently induces high temporal variance between cycles. Finally, Duration Adjustment methods (17, 18) enhance stability by incrementally updating durations, yet they typically rely on fixed linear steps (e.g.,  $\Delta t \in \{0, \pm 3, \pm 6\}$ ). This fixed granularity creates an inherent trade-off: linear steps are often too small to counter sudden congestion surges or too large to maintain steady-state stability.

## PROBLEM FORMULATION

We first define the fundamental structural components of an intersection (shown in Figure 1):

- Incoming and outgoing Lanes ( $l_i$  and  $l'_i$  in Figure 1): The set of lanes carrying traffic approaching or departing from the intersection.
- Movements ( $m$ ): A specific traffic stream transitioning from a subset of incoming lanes to a subset of outgoing lanes. For instance, movement  $m_1$  includes  $l_2$  in Figure 1. Let  $\mathcal{M}$  denote the set of all valid movements at an intersection.
- Phases ( $p$ ): A set of non-conflicting movements that are allowed to proceed simultaneously. For instance, Phase-3 includes  $\{m_1, m_2, m_3, m_4\}$  in Figure 1.

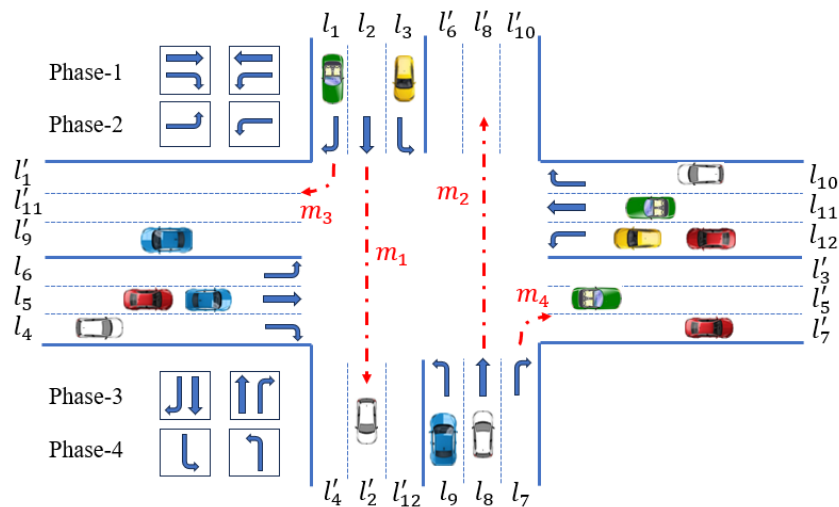


Figure 1: Traffic Terminology

We model the traffic signal control problem across a network of  $N$  intersections as a **Decentralized Partially Observable Markov Decision Process (Dec-POMDP)**. Each intersection oper-

ates as an autonomous agent that interacts with the environment. Formally, the Dec-POMDP is defined by the tuple  $\langle \mathcal{S}, \mathcal{A}, \mathcal{P}, \mathcal{R}, \mathcal{O}, \gamma \rangle$ , where:

- $\mathcal{S}$ : Denotes the global state space of the environment, including real-time traffic distributions and the current signal control status.
- $\mathcal{O}$ : Represents the set of joint observations. Each agent  $i$  receives a local observation  $o_{i,t} \in \mathcal{O}$  derived from the global state  $\mathbf{s}_t$  according to an observation function.
- $\mathcal{A}$ : Represents the set of joint action space. At each time step  $t$ , agents execute a joint action  $\mathbf{a}_t = \{a_{1,t}, \dots, a_{N,t}\} \in \mathcal{A}$ .
- $\mathcal{P}(\mathbf{s}_{t+1}|\mathbf{s}_t, \mathbf{a}_t)$ : Represents the state transition probability function, denoting the probability of the environment transitioning to state  $\mathbf{s}_{t+1}$  by the current state  $\mathbf{s}_t$  and action  $\mathbf{a}_t$ .
- $\mathcal{R}$ : Is the reward function that evaluates the immediate quality of  $\mathbf{a}_t$ , in the form of  $\mathbf{r}_t = \{r_{1,t}, \dots, r_{N,t}\}$ . Common reward designs include throughput or waiting time.
- $\gamma$ :  $\gamma \in [0, 1)$  is the discount factor, which determines the importance of future rewards.

The objective is to maximize the expected return  $J(\pi) = \mathbb{E}[\sum_{i=1}^N \sum_{k=0}^{\infty} \gamma^k r_{i,t+k}]$ , where  $\pi = \{\pi_1, \dots, \pi_N\}$  and  $\pi_i(o_{i,t}) = a_{i,t}$  for the state  $\mathbf{s}_t$  and agent  $i$ . In this paper, we define the state  $\mathbf{s}_t$  as the concatenation of the current phase ID, the time elapsed in this current phase, and a vector of vehicle counts for each lane within a limited range on approaching links, and the reward is computed using a weighted-sum of travel time (s), waiting time (s), average speed (s), and throughput (vehs).

## OBSERVATION SCOPES ANALYSIS

The scope of information available to an agent fundamentally dictates the balance between control efficacy and system scalability. As illustrated in Figure 2 (where the agent controls the central intersection 3), we categorize observation scopes into three distinct levels.

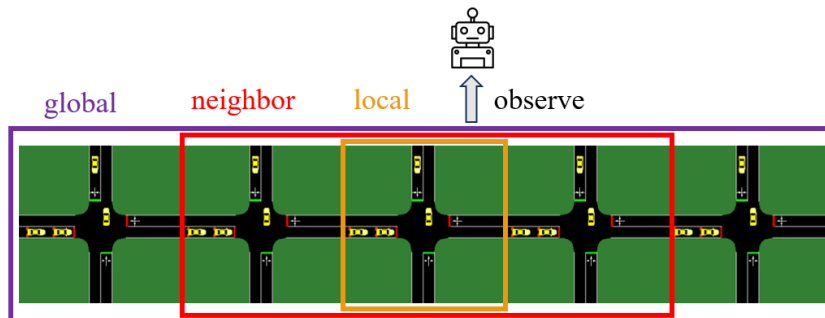


**Figure 2: Observation scope**

First, local observation ( $O^{\text{local}}$ ) restricts visibility to the host intersection. While efficient, this myopia prevents agents from anticipating upstream platoons, hindering green wave formation (19). Conversely, global observation ( $O^{\text{global}}$ ) covers the entire network. Although theoretically optimal, it faces severe scalability issues; the input dimension grows linearly with network size  $|N|$ , yielding an unmanageable complexity of  $O(|N| \times |O^{\text{local}}|)$ . To resolve this, neighbor observation ( $O^{\text{neighbor}}$ ) includes only directly connected intersections  $\mathcal{N}_i$ . This captures essential incoming flow dynamics for coordination while maintaining a constant state space size independent of the total network dimension.

## METHODOLOGY

In this section, we detail the proposed MARL framework designed for real-world traffic signal control deployment. Our methodology focuses on three critical aspects: environmental robust-

ness, control stability, and system scalability.

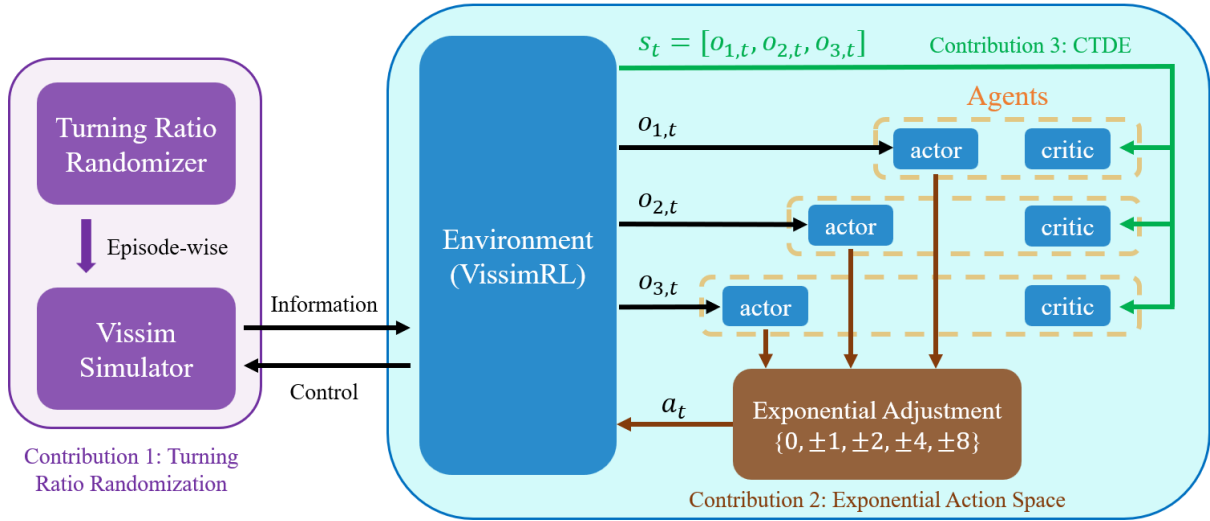


**Figure 3: Method Architecture**

## TURNING RATIO RANDOMIZATION

Traffic dynamics are governed by two distinct factors: *traffic volume*, which dictates the overall intersection load and required cycle length, and *turning ratios*, which fundamentally determine the optimal green split—the allocation of green signal durations among competing phases. In standard RL training environments, both traffic volume and turning ratios remain static. Under such conditions, agents face a significant risk of overfitting. Instead of learning to interpret state observations, they tend to converge toward an ‘open-loop’ policy, implicitly memorizing a fixed timing schedule (e.g., ‘switch phase after 15 seconds’) that aligns with the static accumulation pattern. This results in a brittle policy that fails to react to real-time fluctuations. Conversely, varying traffic volume introduces reward instability. Since metrics like waiting time are highly sensitive to network load, volume fluctuations cause reward magnitudes to shift independent of policy quality. This generates ‘misleading signals’ that can destabilize the learning process.

To counter this, we introduce a **Turning Ratio Randomization** strategy. At the beginning of each training episode, we perturb the turning probabilities of all approaches using a uniform distribution scaling method. Specifically, we apply independent multiplicative noise to each movement’s ratio and subsequently re-normalize the values to ensure the probabilities sum to one. Let  $r_m$  denote the original turning ratio for movement  $m$ . The perturbed ratio  $r'_m$  is computed via the following three steps:

1. Noise Sampling: Sample a noise factor  $\epsilon_m \sim U(-\delta, \delta)$  for each movement, where  $\delta \in [0, 1]$  is a hyperparameter controlling the perturbation intensity.
2. Scaling: Compute the intermediate perturbed ratio:

$$\hat{r}_m = r_m \cdot (1 + \epsilon_m) \quad (1)$$

3. Normalization: Re-normalize to obtain the final turning ratio:

$$r'_m = \frac{\hat{r}_m}{\sum_{k \in \mathcal{M}} \hat{r}_k} \quad (2)$$

This approach ensures that the perturbation remains proportional to the original traffic demand, effectively preventing dominant traffic flows from being disproportionately distorted by additive noise while maintaining realistic structure.

## EXPONENTIAL PHASE DURATION ADJUSTMENT

To ensure safety and smooth traffic flow, we adopt a Cyclic Phase control scheme. Furthermore, in order to match drivers' expectations, within each phase, the order of green, yellow, red shall remain unchanged. Fixed durations are set for yellow and an all-phase red that is meant to clear the intersection. Therefore, the core innovation lies in how the green duration of the next phase in the cycle is determined. We propose an **Exponential Phase Duration Adjustment** to achieve "coarse-to-fine" control granularity.

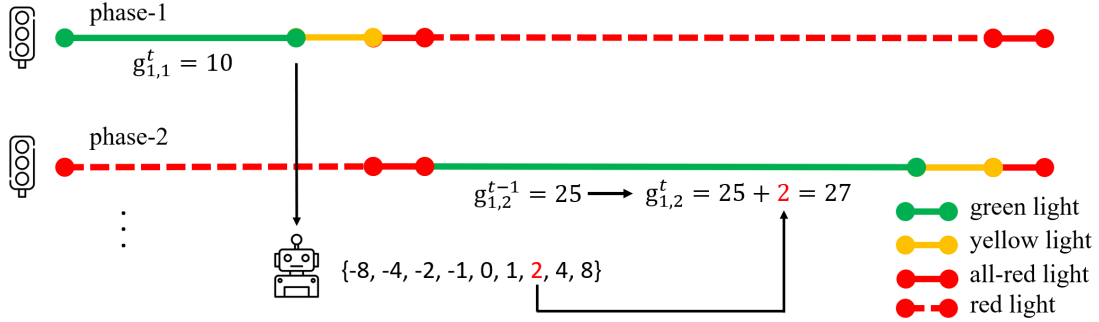


**Figure 4: Action space: Set Next Phase Duration with small change**

Let  $g_{i,p}^t$  be the green light duration for phase  $p$  at intersection  $i$  during cycle  $t$ . The agent selects an adjustment action  $\Delta t$  from a discrete exponential adjustment set:

$$\Delta t \in \{0, \pm\lambda^0, \pm\lambda^1, \pm\lambda^2, \pm\lambda^3\} \quad (3)$$

where  $\lambda$  is a hyperparameter that determines the granularity of the adjustment. The duration for the next cycle is determined at the end of the previous phase as:

$$g_{i,p}^t = \text{clip}(g_{i,p}^{t-1} + \Delta t, g_{\min}, g_{\max}) \quad (4)$$

where  $g_{i,p}^t$  is constrained by the minimum and maximum green times  $g_{\min}$  and  $g_{\max}$ .

In Linear Adjustment methods, short intervals will allow finer control, but require multiple cycles when large adjustments are needed. In contrast, long intervals allow for rapid, flexible adjustment at the expense of finer control. By integrating an exponential scale, we can enjoy both benefits with no downsides. The larger steps (e.g.,  $\pm 8$ s if  $\lambda = 2$ ) provide the necessary agility to counteract sudden congestion, while the finer granularity (e.g., 0s or  $\pm 1$ s) ensures precise timing during steady states. Consequently, the control policy maintains smooth progression in normal conditions without sacrificing the responsiveness required for critical traffic events.

## SCALABLE COORDINATION VIA NEIGHBOR-LEVEL OBSERVATION

For large-scale network control, we must make the choice between global observation, which is optimal but unscalable, or local observation, which is scalable but myopic. To bridge this gap, we propose using neighbor-level observation empowered by the Centralized Training Decentralized Execution (CTDE) paradigm.

CTDE fundamentally decouples the information scope available during learning from that which is restricted during deployment. In the training stage, a centralized critic exploits global information, incorporating the joint states of all agents across the entire network, to accurately evaluate the network-wide impact of local actions. During execution, each agent functions as a decentralized actor, inferring optimal policies based solely on partial observations.

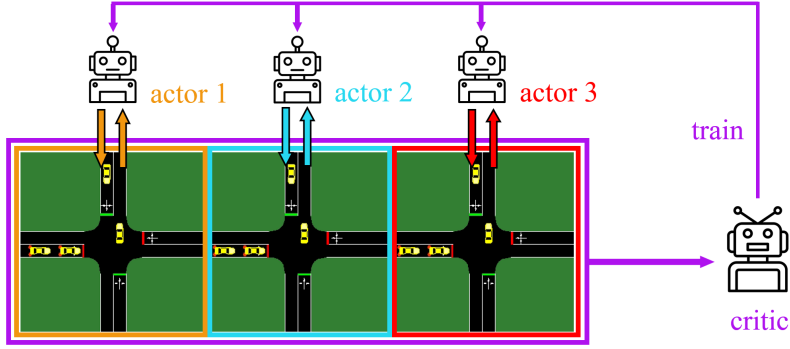


**Figure 5: CTDE Paradigm**

We define the observation scope  $\mathcal{O}^{\text{neighbor}}$  for each agent to include its local observation and the aggregated information from directly connected upstream and downstream neighbors  $\mathcal{N}_i$ :

$$o_{i,t}^{\text{neighbor}} = \{o_{i,t}^{\text{local}}\} \cup \{o_{j,t}^{\text{local}} \mid j \in \mathcal{N}_i\} \quad (5)$$

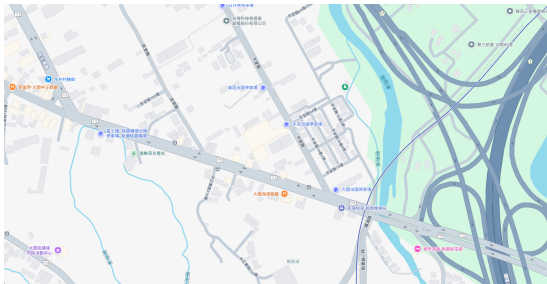
To implement this framework, we adopt the Multi-Agent Proximal Policy Optimization (MAPPO) algorithm (20). It combines the stability of PPO’s trust-region updates with the CTDE framework. This mechanism enables agents to internalize cooperative behaviors and anticipate network-wide impacts, effectively achieving global coordination performance within a scalable, decentralized architecture.

## EXPERIMENTS

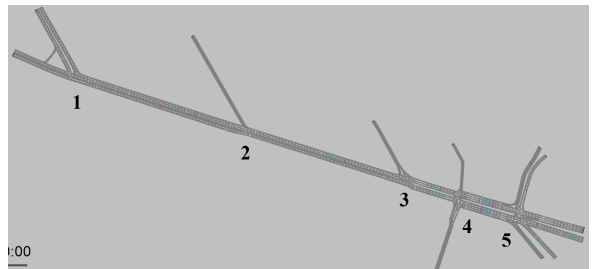
This section empirically validates the effectiveness and stability of the proposed MARL framework. We detail the experimental setup, present quantitative comparisons and ablation studies, and conclude with a qualitative stability analysis.

### EXPERIMENTAL SETTINGS

**Simulation Environment and Road Network** To ensure practical relevance and fidelity, we utilize PTV Vissim, a microscopic simulator employing the psycho-physical Wiedemann car-following model (21). Vissim accurately captures the stochastic dynamics of human driving behavior, serving as a robust testbed for sim-to-real validation. The simulation environment is a calibrated digital twin of Zhongzheng East Road in Taoyuan City, Taiwan, comprising five consecutive signalized intersections characterized by short spacing and high interaction (Figure 6). Network geometry, including lane configurations and turning pockets, was rigorously aligned with real-world satellite imagery and field surveys.



(a) Satellite Image



(b) Vissim Modeling

**Figure 6: Experimental Network**

**Traffic Data and Scenarios** A critical challenge in RL research is the bias introduced by using

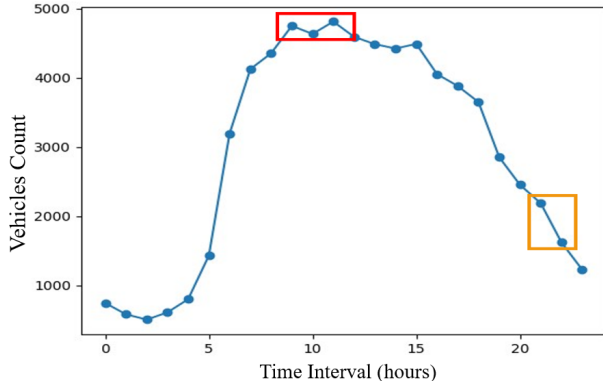


**Figure 7: 24-hour traffic volume**

*Note.* This 24-hour weekday count tracks vehicles entering the source link.

**Table 1: Traffic volume**

| Flow      | Data Time   | Vehicle Count (vehs/hr) |
|-----------|-------------|-------------------------|
| Peak Hour | 9:00-10:00  | ~ 4800                  |
| Off-Peak  | 21:00-22:00 | ~ 1800                  |

identical traffic distributions for training and testing. To mitigate this, we implemented a cross-scenario validation mechanism. We analyzed 24-hour real-world detector data (Figure 7) to extract two distinct stress levels: a high-load peak hour and a moderate-load off-peak hour (Table 1). This paper only considers four-wheeled vehicles. Agents are trained strictly on peak hour data to enforce policy optimization under high-pressure conditions, while evaluation is conducted on both scenarios to test generalization.

**Comparative Methods** For comparative analysis, we benchmark our framework against a fixed-time plan optimized for green waves and the MaxPressure heuristic (22). We evaluate our proposed methods using a unified notation  $M_{scope}^{strategy}$ , where the subscript denotes the observation scope (local, neighbor, global) and the superscript indicates the training strategy (static, randomized).

**Evaluation Metrics** Following established evaluation protocols in recent TSC review (23), we quantify performance using four metrics: Average Travel Time (ATT, s/veh), Average Waiting Time (AWT, s/veh), Average Delay (AD, s/veh), and Vehicle Count (VC, vehs/h).

## EXPERIMENTAL RESULTS AND ANALYSIS

Table 2 presents the quantitative comparison of all methods across the four evaluation metrics under both peak and off-peak scenarios. The results reveal distinct performance patterns regarding robustness and generalization.

In the peak hour scenario (Table 2 left), which aligns with the training distribution, the proposed MARL framework demonstrates superior control efficiency compared to the baselines. Specifically, the robustly trained  $M_{neighbor}^{randomized}$  achieves an ATT of 230.58s, significantly surpassing the competitive MaxPressure heuristic (265.79s). This confirms that our framework effectively learns efficient signal timing policies under high-congestion conditions.

The off-peak scenario (Table 2 right) serves as a critical test for generalization and highlights the impact of the training strategy. Results also reveal that standard RL models trained with static ratios fail to adapt to this unseen environment. Due to severe overfitting to specific training patterns, their performance degrades significantly, falling even behind the heuristic baselines. In contrast, Turning Ratio Randomization significantly enhances robustness. While the global-view agent  $M_{global}^{randomized}$  naturally achieves the best performance (119.32s ATT), the neighbor-based agent  $M_{neighbor}^{randomized}$  also performs remarkably well (124.37s ATT). It not only outperforms

**Table 2: Performance Comparison between Peak and Off-Peak Scenarios**

| Category         | Method                                    | Peak Hour Flow |               |               |                | Off-Peak Hour Flow |              |              |                |
|------------------|---|----------------|---------------|---------------|----------------|--------------------|--------------|--------------|----------------|
|                  |   | ATT ↓          | AWT ↓         | AD ↓          | VC ↑           | ATT ↓              | AWT ↓        | AD ↓         | VC ↑           |
| Baseline         | FixTime                                   | 383.92         | 352.87        | 319.04        | 4015.87        | 129.20             | 50.74        | 58.60        | 1789.93        |
|                  | MaxPressure                               | 265.79         | 285.93        | 196.54        | 4223.80        | 126.57             | 45.96        | 55.82        | 1797.53        |
| Standard RL      | $M_{\text{local}}^{\text{static}}$        | 266.07         | 227.79        | 197.74        | 4446.93        | 132.20             | 51.42        | 61.32        | 1799.80        |
|                  | $M_{\text{neighbor}}^{\text{static}}$     | 249.54         | <b>215.47</b> | 181.08        | <b>4448.13</b> | 130.27             | 50.02        | 59.59        | 1798.53        |
|                  | $M_{\text{global}}^{\text{static}}$       | 262.24         | 230.62        | 194.05        | 4404.20        | 135.71             | 51.46        | 65.05        | 1787.20        |
| Robust RL (ours) | $M_{\text{local}}^{\text{randomized}}$    | 242.96         | 228.36        | 174.44        | 4316.80        | 129.37             | 48.05        | 58.47        | 1801.47        |
|                  | $M_{\text{neighbor}}^{\text{randomized}}$ | <b>230.58</b>  | 231.01        | <b>160.34</b> | 4416.53        | 124.37             | 44.09        | 53.44        | <b>1808.47</b> |
|                  | $M_{\text{global}}^{\text{randomized}}$   | 256.39         | 219.30        | 188.08        | 4398.80        | <b>119.32</b>      | <b>36.12</b> | <b>48.33</b> | 1802.80        |

**Table 3: non-CTDE Algorithm v.s. CTDE Algorithm**

| Category | Algorithm   | Peak Hour Flow |               |               |                | Off-Peak Hour Flow |              |              |                |
|----------|-------------|----------------|---------------|---------------|----------------|--------------------|--------------|--------------|----------------|
|          |             | ATT ↓          | AWT ↓         | AD ↓          | VC ↑           | ATT ↓              | AWT ↓        | AD ↓         | VC ↑           |
| Baseline | FixTime     | 383.92         | 352.87        | 319.04        | 4015.87        | 129.20             | 50.74        | 58.60        | 1789.93        |
|          | MaxPressure | 265.79         | 285.93        | 196.54        | 4223.80        | 126.57             | 45.96        | 55.82        | 1797.53        |
| RL-based | non-CTDE    | 298.43         | 319.72        | 231.89        | 4124.13        | 134.20             | 52.08        | 63.40        | 1790.20        |
|          | CTDE (ours) | <b>230.58</b>  | <b>231.01</b> | <b>160.34</b> | <b>4416.53</b> | <b>124.37</b>      | <b>44.09</b> | <b>53.44</b> | <b>1808.47</b> |

the MaxPressure baseline (126.57s ATT) but also approaches the efficacy of the global agent.

Ultimately, this underscores the pivotal role of Turning Ratio Randomization as an essential regularization technique, equipping the agent with the necessary robustness to function reliably in dynamic, unseen environments where standard training falls short.

## COMPONENT ANALYSIS

To provide a deeper analysis of our framework’s internal mechanisms, this section conducts targeted ablation studies on critical design choices.

First, we assess the necessity of the CTDE paradigm by benchmarking MAPPO against the non-CTDE algorithm IPPO. For a fair comparison, both algorithms utilize identical Neighbor-Level Observations and Turning Ratio Randomization, differing solely in their critic mechanism: IPPO uses a decentralized critic, whereas MAPPO employs the centralized critic.

As shown in Table 3, MAPPO significantly outperforms IPPO. While IPPO suffers from environment non-stationarity and unstable credit assignment due to simultaneous neighbor updates, MAPPO leverages its global critic to guide local actors toward cooperative behaviors, thereby justifying the adoption of the CTDE framework.

Next, we evaluate the efficacy of the proposed action space design by comparing it against Linear Adjustment schemes. We tested two variants of Linear Adjustment: a standard setting  $\{0, \pm 2, \pm 4, \pm 6, \pm 8\}$  and an extended linear set  $\{0, \pm 5, \pm 10, \pm 15, \pm 20\}$  matched to the same action space size (9 actions) as our method. Results (Table 4) indicate that our Exponential Adjustment yields superior performance across all metrics. Although Linear Adjustments can outperform the Fixed-Time plan in peak hours, they degrade significantly in off-peak scenarios.

**Table 4: Action Space Adjustment Comparison**

| Category    | Adjustments   | Peak Hour Flow |               |               |                | Off-Peak Hour Flow |              |              |                |
|-------------|---------------|----------------|---------------|---------------|----------------|--------------------|--------------|--------------|----------------|
|             |               | ATT ↓          | AWT ↓         | AD ↓          | VC ↑           | ATT ↓              | AWT ↓        | AD ↓         | VC ↑           |
| Baseline    | FixTime       | 383.92         | 352.87        | 319.04        | 4015.87        | 129.20             | 50.74        | 58.60        | 1789.93        |
|             | MaxPressure   | 265.79         | 285.93        | 196.54        | 4223.80        | 126.57             | 45.96        | 55.82        | 1797.53        |
| Linear      | Small-Scale   | 263.11         | 289.70        | 196.79        | 4226.00        | 158.10             | 73.18        | 87.64        | 1775.87        |
|             | Large-Scale   | 283.56         | 267.24        | 216.80        | 4229.60        | 144.96             | 59.32        | 74.09        | 1793.33        |
| Exponential | Base-2 (ours) | <b>230.58</b>  | 231.01        | <b>160.34</b> | 4416.53        | <b>124.37</b>      | 44.09        | <b>53.44</b> | <b>1808.47</b> |
|             | Base-3 (ours) | 234.36         | <b>215.12</b> | 165.06        | <b>4445.80</b> | 125.98             | <b>43.11</b> | 54.86        | 1801.40        |

Note: Linear: Small-Scale {0, ±2, ±4, ±6, ±8}, Large-Scale {0, ±5, ±10, ±15, ±20}; Exponential: Base-2 {0, ±1, ±2, ±4, ±8}, Base-3 {0, ±1, ±3, ±9, ±27}

In contrast, the exponential distribution concentrates fine-grained actions near zero to minimize oscillation during stable flows, while simultaneously retaining large-magnitude actions to rapidly dissipate sudden queues. Consequently, the exponential design effectively balances the need for large-scale adjustments during congestion with the precision required for stable traffic.

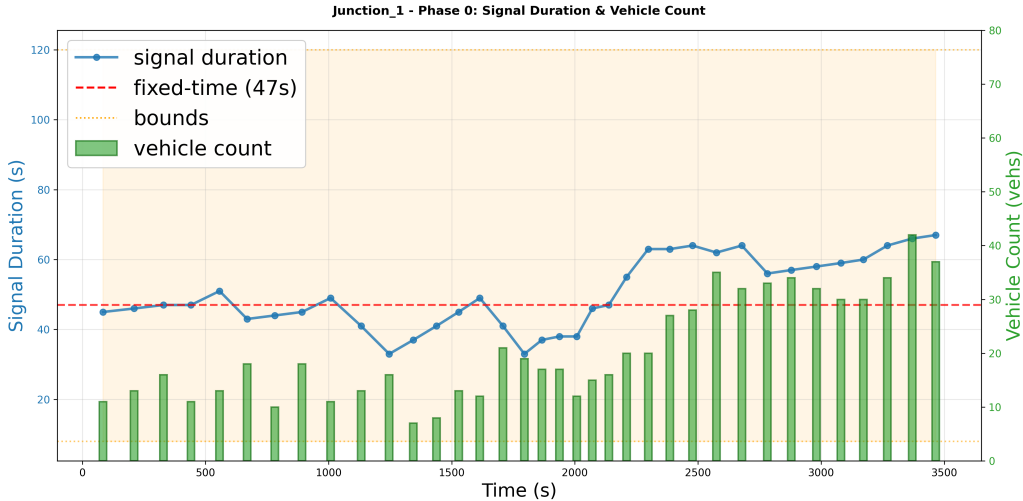


**Figure 8: Synchronization of Signal Supply and Traffic Demand.**

Note: The blue line and green bars track RL signal duration and traffic demand, respectively, for the primary phase in the busiest intersection. The red dashed line marks the fixed duration baseline of 47s. All durations fall within the yellow feasible action space.

Finally, to validate the model’s responsiveness to traffic dynamics, we analyze the temporal correlation between signal duration and traffic volume. We specifically selected the intersection with the highest traffic volume, comparing the green time allocated to its primary phase against the vehicle count on the corresponding critical lane on main links. As shown in Figure 8, our method exhibits strong adaptability. The agent dynamically scales signal duration to match real-time demand—reducing green time during low-traffic periods and extending it during congestion—thereby confirming its capability to handle dynamic traffic patterns.

## CONCLUSION

This paper addresses the critical challenges of robustness, stability, and scalability in applying DRL to real-world Traffic Signal Control. We proposed a high-fidelity MARL framework

integrating three key innovations: Turning Ratio Randomization, Exponential Phase Duration Adjustment, and Neighbor-Based CTDE. Experimental results confirm that our randomization strategy effectively prevents overfitting by enforcing state-based reactivity. Furthermore, the CTDE paradigm successfully resolves the scalability-optimality dilemma, enabling agents with limited neighbor observations to achieve global-level coordination. By bridging the sim-to-real gap, this work offers a viable path for deploying autonomous signal control. Future research will extend this framework to grid networks and incorporate multi-modal traffic data to further enhance urban mobility.

## ACKNOWLEDGEMENT

This work was supported in part by the National Science and Technology Council (NSTC) of Taiwan under Grant, NSTC 114-2221-E-A49-005, NSTC 114-2221-E-A49-006, and in part by ELAN Microelectronics Corporation, Taiwan.

## REFERENCES

- (1) “Global Traffic Scorecard-INRIX Global Traffic Ranking,” Available at <https://inrix.com/scorecard/>.
- (2) Krajzewicz, D., Hertkorn, G., Feld, C., and Wagner, P., *SUMO (Simulation of Urban MObility); An Open-Source Traffic Simulation*, Jan. 2002.
- (3) Zhang, H. *et al.*, “CityFlow: A Multi-Agent Reinforcement Learning Environment for Large Scale City Traffic Scenario,” in *The World Wide Web Conference*, May 2019, pp. 3620–3624.
- (4) “Traffic Simulation Software | PTV Vissim | PTV Group,” Available at <https://www.ptvgroup.com/en/products/ptv-vissim>.
- (5) Chang, H.-C., Huang, S.-Y., Chen, Y.-C., and Wu, I.-C., “VissimRL: A Multi-Agent Reinforcement Learning Framework for Traffic Signal Control Based on Vissim,” in *IEEE Intelligent Vehicles Symposium (IV)*, *arXiv:2601.18284*, Jun. 2026.
- (6) Zang, X., Yao, H., Zheng, G., Xu, N., Xu, K., and Li, Z., “MetaLight: Value-Based Meta-Reinforcement Learning for Traffic Signal Control,” *Proceedings of the AAAI Conference on Artificial Intelligence*, vol. 34, no. 01, pp. 1153–1160, Apr. 2020.
- (7) Ye, Y., Ding, J., Wang, T., Zhou, J., Wei, X., and Chen, M., “FairLight: Fairness-Aware Autonomous Traffic Signal Control With Hierarchical Action Space,” *IEEE Transactions on Computer-Aided Design of Integrated Circuits and Systems*, vol. 42, no. 8, pp. 2434–2446, Aug. 2023.
- (8) Wei, H. *et al.*, “PressLight: Learning Max Pressure Control to Coordinate Traffic Signals in Arterial Network,” in *Proceedings of the 25th ACM SIGKDD International Conference on Knowledge Discovery & Data Mining*, ser. KDD ’19. New York, NY, USA: Association for Computing Machinery, Jul. 2019, pp. 1290–1298.
- (9) Wei, H. *et al.*, “CoLight: Learning Network-level Cooperation for Traffic Signal Control,” in *Proceedings of the 28th ACM International Conference on Information and Knowledge Management*, Nov. 2019, pp. 1913–1922.

- (10) Oroojlooy, A., Nazari, M., Hajinezhad, D., and Silva, J., “AttendLight: Universal Attention-Based Reinforcement Learning Model for Traffic Signal Control,” Oct. 2020.
- (11) Chen, C. *et al.*, “Toward A Thousand Lights: Decentralized Deep Reinforcement Learning for Large-Scale Traffic Signal Control,” *Proceedings of the AAAI Conference on Artificial Intelligence*, vol. 34, no. 04, pp. 3414–3421, Apr. 2020.
- (12) Cabrejas-Egea, A., Zhang, R., and Walton, N., “Reinforcement Learning for Traffic Signal Control: Comparison with Commercial Systems,” *Transportation Research Procedia*, vol. 58, pp. 638–645, Jan. 2021.
- (13) Kumarasamy, V. K. *et al.*, “Integration of Decentralized Graph-Based Multi-Agent Reinforcement Learning with Digital Twin for Traffic Signal Optimization,” *Symmetry*, vol. 16, no. 4, Apr. 2024.
- (14) Zhou, P., Chen, X., Liu, Z., Braud, T., Hui, P., and Kangasharju, J., “DRLE: Decentralized Reinforcement Learning at the Edge for Traffic Light Control in the IoV,” *IEEE Transactions on Intelligent Transportation Systems*, vol. 22, no. 4, pp. 2262–2273, Apr. 2021.
- (15) Zhang, Z. *et al.*, “Phase Re-service in Reinforcement Learning Traffic Signal Control,” Aug. 2024.
- (16) Park, J., Zhang, G., Wang, C., Wang, H., and Jiang, Z.-P., “Integrated Routing and Traffic Signal Control for CAVs via Reinforcement Learning Approach,” in *2024 IEEE 27th International Conference on Intelligent Transportation Systems (ITSC)*, Sep. 2024, pp. 558–563.
- (17) Wang, M. *et al.*, “Traffic Signal Cycle Control with Centralized Critic and Decentralized Actors under Varying Intervention Frequencies,” *IEEE Transactions on Intelligent Transportation Systems*, vol. 25, no. 12, pp. 20 085–20 104, Dec. 2024.
- (18) Shah, K. D., Patel, D. K., Raval, M. S., Zaveri, M., and Merchant, S., “Deep RL-Based Smart Signaling Using Space-Time Vehicular Features Under C-V2X Scenario,” in *2024 16th International Conference on COMMunication Systems & NETworks (COMSNETS)*, Jan. 2024, pp. 240–245.
- (19) Han, T., Lyu, S., and Oguchi, T., “WaveLearner: A Knowledge-Combined Reinforcement Learning to Understand Coordinated Traffic Signal Control along Urban Arteries,” in *2022 IEEE 25th International Conference on Intelligent Transportation Systems (ITSC)*. Macau, China: IEEE Press, Oct. 2022, pp. 1167–1174.
- (20) Yu, C. *et al.*, “The Surprising Effectiveness of PPO in Cooperative, Multi-Agent Games,” Nov. 2022.
- (21) Wiedemann, R., “SIMULATION DES STRASSENVERKEHRSFLUSSES.” 1974.
- (22) Varaiya, P., “Max pressure control of a network of signalized intersections,” *Transportation Research Part C: Emerging Technologies*, vol. 36, pp. 177–195, Nov. 2013.
- (23) Noaen, M. *et al.*, “Reinforcement learning in urban network traffic signal control: A systematic literature review,” *Expert Systems with Applications*, vol. 199, p. 116830, Aug. 2022.